RSC Advances

PAPER

View Article Online
View Journal | View Issue

Cite this: *RSC Adv.*, 2023, **13**, 3612

Construction of a $Bi_2WO_6/BiVO_4$ photocatalytic system for efficient visible light degradation of tetracycline drugs†

Yiyao Zhang,‡[a] Hongchen Song,‡[ab] Jintai Han,[a] Yunchao Liu,[a] Jing Sun,*[a] Tingting Shen,*[a] Xikui Wang,[c] Zhen Wang,[b] Weizhen Zhang[a] and Xuerui Yao[a]

A $Bi_2WO_6/BiVO_4$ composite photocatalytic material was synthesized by the hydrothermal method, and achieved the effective degradation of oxytetracycline (OTC) and tetracycline (TC) under visible light. The compositions, structures, chemical states and optoelectronic properties of Bi_2WO_6, $BiVO_4$ and $Bi_2WO_6/BiVO_4$ composites were characterized by systematic characterization. The results show that the existence of the heterojunction interface facilitates the separation of photogenerated carriers. Compared with the pure catalyst of Bi_2WO_6 and $BiVO_4$, the $Bi_2WO_6/BiVO_4$ composite material significantly improves the degradation efficiency of OTC and TC. The degradation rate is 6.22 and 3.02 times higher than that of Bi_2WO_6 and $BiVO_4$, respectively. Through the free radical quenching experiments, it is known that photogenerated holes (h^+) and superoxide anion free radicals ($\cdot O_2^-$) are the main active substances in the degradation of OTC. By analyzing the process of photocatalytic degradation of OTC, there are mainly six intermediates during the process. Their possible degradation pathways are also inferred in this paper.

Received 23rd November 2022
Accepted 20th January 2023

DOI: 10.1039/d2ra07460e

rsc.li/rsc-advances

1. Introduction

Tetracyclines are the earliest broad-spectrum antibiotics and have been widely used in medical, animal husbandry and other industries since their invention in 1948.[1,2] Their structures all contain the basic framework of tetracene, and the main types include tetracycline (TC), oxytetracycline (OTC), chlorotetracycline and semi synthetic derivative doxycycline.[3,4] They have antibacterial effects on common rickettsia and anaerobic bacteria, mycoplasma and some protozoa.[5] However, since they have been used for a long time and on a large scale, the concentration of residual tetracyclines in the environment has continued to rise, increasing the resistance of pathogenic microorganisms and causing serious harm to the ecological balance and human health.[6,7] These negative effects are reflected in the production of resistant strains, which reduces the antibacterial performance of antibiotics.[8,9] Residual antibiotics can enter the human body through the food chain and food web and affect the immune system.

The traditional antibiotic removal methods have certain shortcomings. For example, the physical methods represented by adsorption and reverse osmosis only transfer antibiotics from the aqueous phase to another phase, thereby failing to solve the toxicity problem.[10,11] This still cause secondary pollution in the environment. The biological treatment of antibiotic wastewater has strict requirements on the wastewater environment, such as nutrient composition, pH, temperature and others. The unqualified wastewater environment will lead to the inactivation of microorganisms and affect the degradation efficiency.[12] The chemical method involves the addition of oxidant to produce strong oxidation group has high cost and can easily cause secondary pollution.[13]

Photocatalytic treatment technology uses sunlight,[14,15] which is a renewable energy source, as its energy source to generate active free radicals in the catalytic system for decomposing pollutants into small molecules, such as carbon dioxide and water.[16,17] In addition, photocatalytic technology also has the advantages of high mineralization, non-toxic and high stability.[3,18] Therefore, photocatalytic treatment of antibiotics in wastewater is an effective method,[19,20]and this technology has a wide research potential in the environmental field.[21,22]

Bi_2WO_6 is a typical n-type semiconductor photocatalyst material with perovskite lamellar structure. Considering its convenient synthesis, unique photoelectric performance and catalysis, it has attracted extensive attention.[23] Although

[a]*School of Environmental Science and Engineering, Qilu University of Technology (Shandong Academy of Sciences), Jinan 250353, PR China. E-mail: sunjing77@qlu.edu.cn; shentingting@qlu.edu.cn*

[b]*Shangdong Haijingtian Environmental Protection Technology Stock Company, Binzhou 256600, PR China*

[c]*College of Environmental Science and Engineering, Shandong Agriculture and Engineering University, Jinan 251100, PR China*

† Electronic supplementary information (ESI) available. See DOI: https://doi.org/10.1039/d2ra07460e

‡ These authors contributed equally to the work.

Bi_2WO_6 can absorb visible light, it has the disadvantages of low quantum efficiency and high recombination rate of photogenerated carriers, which greatly limits its practical application.[24,25] To improve the photocatalytic activity of Bi_2WO_6, various improvement strategies have been proposed, including metal and nonmetal element doping and heterostructure construction. However, it has been shown that elemental doping decreases the carrier migration and leads to doping energy level dispersion,[26] and the dopant also acts as a complex center for carriers,[27] which was not conducive to the improvement of photocatalytic activity. The preparation of heterojunctions has been shown to be an effective method to promote charge separation.[28,29] Coupling Bi_2WO_6 with narrow bandgap semiconductors to form heterojunctions also can effectively extend the light absorption range.[30] $BiVO_4$ was reported to be a promising visible photocatalyst, which was widely used for the removal of organic pollutants from wastewater due to its excellent optical and electronic properties and narrow bandgap energy.[31,32] In addition, $BiVO_4$ has an energy band edge matching Bi_2WO_6, so $BiVO_4$ was introduced to build heterostructures.[33]

In this study, $Bi_2WO_6/BiVO_4$ heterojunction materials were constructed by hydrothermal method for the degradation of OTC and TC. The structure, composition, morphology and optoelectronic properties of the materials were investigated by systematic characterization. To understand the potential applications of the materials in real-world environments, the effects of common anions on the photocatalytic degradation of OTC were investigated. The degradation mechanism of $Bi_2WO_6/BiVO_4$ composites was proposed by free radical burst experiments. The degradation intermediates were analyzed in combination with high performance liquid–liquid mass spectrometry (LC-MS) technique, and possible degradation pathways of OTC were proposed.

2. Experiment part

2.1 Experimental materials

Bismuth chloride ($BiCl_3$,AR) was purchased from Shanghai Macklin Biochemical Technology Co. Ltd. Ammonium metavanadate (NH_4VO_3,AR) was purchased from Xilong Science Co. Ltd. Ethanolamine (C_2H_7NO, AR) was purchased from Shanghai Aladdin Biochemical Technology Co. Ltd. Formic acid (HCOOH) was purchased from Comio Chemical Reagent Co. Ltd. Cetyltrimethylammonium bromide (CTAB), sodium tungstate dihydrate ($Na_2WO_4 \cdot 2H_2O$, AR), absolute ethanol, *tert*-butanol (*t*-butanol), methanol, acetonitrile, bismuth nitrate pentahydrate ($Bi(NO_3)_3 \cdot 5H_2O$, AR) and sodium sulfate (Na_2SO_4) were all purchased from Sinopharm Chemical Reagents Co. Ltd.

2.2 Material preparation

2.2.1 Preparation method of $BiVO_4$. 0.632 g of $BiCl_3$ was weighed and dissolved in 200 mL of deionized water and dispersed evenly under magnetic stirring. NH_4VO_3 (0.236 g) was added and stirred for 30 min, and the color changed from white to light brown. Then, 1.2 mL of 1 mol L^{-1} C_2H_7NO solution was added to mix the solution uniformly by ultrasonic for 60 min, and the color changed from light brown to dark brown. Finally, the solution was poured into a hydrothermal reactor made of polytetrafluoroethylene and kept at 160 °C for 12 h. After cooling to room temperature, the solution was washed with absolute ethanol and deionized water for several times to remove impurities, and a yellow solid (BVO) was obtained. This solid was dried overnight at 60 °C.

2.2.2 Preparation of Bi_2WO_6. 0.1 g of CTAB was dissolved in 160 mL of deionized water, and stirred to disperse evenly. Then, 2 mmol of $Na_2WO_4 \cdot 2H_2O$ and 4 mmol of Bi $(NO_3)_3 \cdot 5H_2O$ was added and stirred vigorously for 120 min, and the solution was transferred to a hydrothermal reactor and heated at 120 °C for 24 h. After natural cooling, the white precipitate was washed with deionized water for several times and then freeze dried overnight to obtain Bi_2WO_6 material (BWO).

2.2.3 Preparation of $Bi_2WO_6/BiVO_4$ composite materials. 40 mL deionized water and 40 mL absolute ethanol were mixed; then, 0.5 g of the sum of the two materials was added, of which Bi_2WO_6 accounted for 5%, 10%, 20%, and 33% of the total mass. After stirring for 1 h and ultrasonic treatment for 30 min, it was transferred to the inner lining of the reactor and kept at 120 °C for 6 h. The obtained material was washed several times and dried at 60 °C for 12 h. The numbers of the obtained $Bi_2WO_6/BiVO_4$ were 5% W/BVO, 10% W/BVO, 20% W/BVO, and 33% W/BVO.

2.3 Characterization of $Bi_2WO_6/BiVO_4$

The instrument used for XRD is X-ray diffractometer (SmartLab SE); it uses Kα ray at a scanning speed of 0.02° per s. The instrument used for SEM is field emission scanning electron microscope ZEISS GEMINI 500. The instrument used in XPS is an X-ray photoelectron spectrometer (ESCALABXi+) calibrated with C 1s = 284.8 eV. The instrument used for UV-Vis DRS is Shimadzu UV-3600 Plus, Japan, with a detection range of 200–800 nm. The instrument used for photoluminescence (PL) spectrum is Edinburgh FLS1000, and the excitation wavelength is 295 nm. The instrument used for photocurrent is Shanghai Chenhua Electrochemical Workstation CHI 600E.

Measuring method of photocurrent: 10 mg of material was added to 1 mL of mixed solution (ethanol : Nafion = 9 : 1) for ultrasonic dispersion for 1 h to obtain suspension. The suspension at 0.3 mL was slowly dropped to 2 × 2 cm^2 of ITO conductive glass and dried at 50 °C for 6 h for standby. A three-electrode system was adopted. Ag/AgCl electrode was the reference electrode, ITO conductive glass coated with material was the working electrode, the electrolyte was 0.1 mol L^{-1} sodium sulfate solution.

2.4 Study on the degradation of tetracyclines by $Bi_2WO_6/BiVO_4$

Taking OTC and TC as target pollutants and by using filters (λ > 400 nm) as a visible light source, the catalytic activity of photocatalytic materials was studied.

The specific experimental steps for the photocatalytic degradation of OTC (or TC) were as follows. Photocatalyst

material (0.01 g) was added into the OTC (or TC) solution containing 100 mL (20 ppm) and stirred for 30 min under dark conditions. Then, a xenon lamp was used for irradiation. Samples were collected at fixed intervals and filtered using a 0.45 μm filter tip.

The liquid phase detection conditions of OTC (TC) are as follows. The chromatographic column was Hypersil GOLD C18, the detection wavelength was 360 nm (355 nm), the mobile phase were formic acid solution (concentration 0.2%) and methanol (V : V = 75 : 25), the flow rate set at 1.2 mL min^{-1}, and the amount of sample injected each time was 20 μL. The temperature of the column temperature box was 35 °C. The degradation rate of OTC (TC) was calculated according to eqn S(1).†

The degradation products of OTC were analyzed by Brooke's high resolution mass spectrometry. The liquid chromatographic column was ACQUITY UPLC HSS T3 1.8 μm. The mobile phases were formic acid solution (concentration 0.1%) and acetonitrile. The elution gradient started from 5% acetonitrile, rose to 100% at 20 min and was maintained for 5 min, and the percentage of acetonitrile decreased to 5% at 25.1 min and stabilized for 4.9 min before returning to the initial percentage.

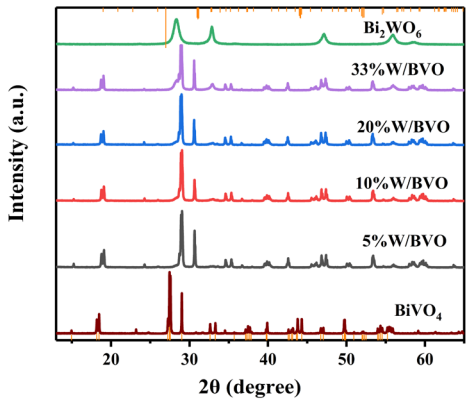

Fig. 1 XRD patterns of $BiVO_4$, Bi_2WO_6, and $Bi_2WO_6/BiVO_4$.

3. Results and discussion

3.1 Characterization of catalysts

3.1.1 X-ray diffraction (XRD) analysis. Fig. 1 shows the XRD spectrum of the prepared sample, the characteristic diffraction peaks of $BiVO_4$ at 2θ = 15.1°, 19.0°, 28.9°, 30.5°, 34.5°, 39.8°, 42.5°, 47.3°, 50.3°, 53.2° corresponded to the (020), (011), (121), (040), (200), (211), (051), (042), (202), and (−161) crystal faces in monoclinic scheelite phase of $BiVO_4$ (JCPDS no. 14-0688), respectively.[34] In the spectrum of Bi_2WO_6, 2θ = 28.3°, 32.8°, 47.2°, 55.8°, 58.6° corresponded to (113), (200), (220), (313), and (226) crystal faces in Bi_2WO_6 (JCPDS no. 73-1126), respectively.[35] After the two compounds were combined, the XRD spectrum of $Bi_2WO_6/BiVO_4$ was dominated by the characteristic diffraction

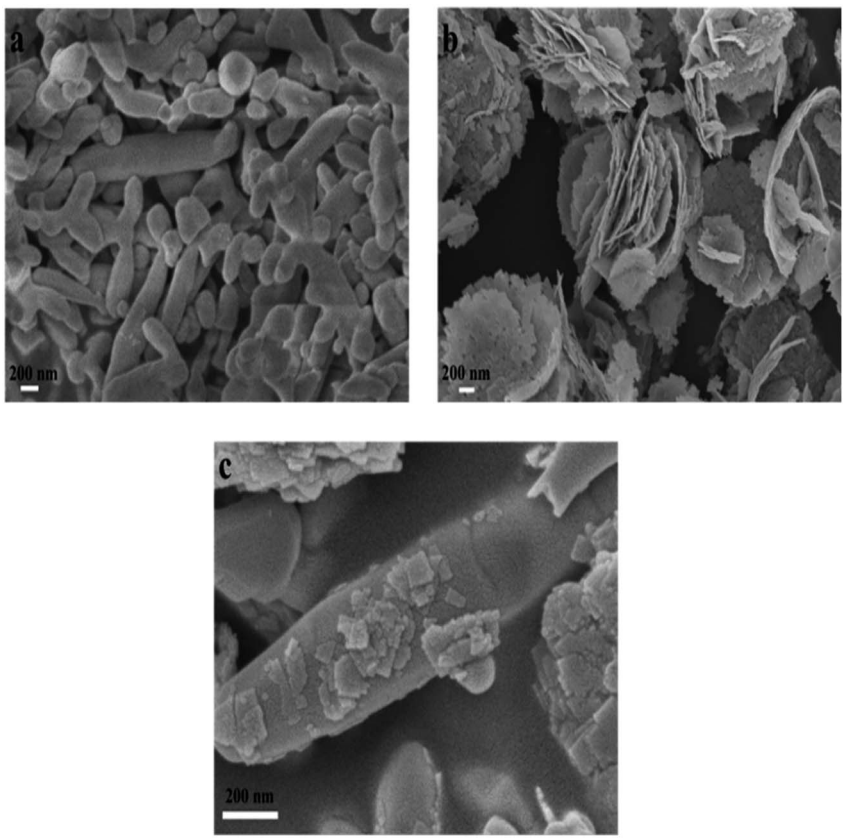

Fig. 2 SEM spectrum of (a) $BiVO_4$, (b) Bi_2WO_6, and (c) 10% W/BVO composites.

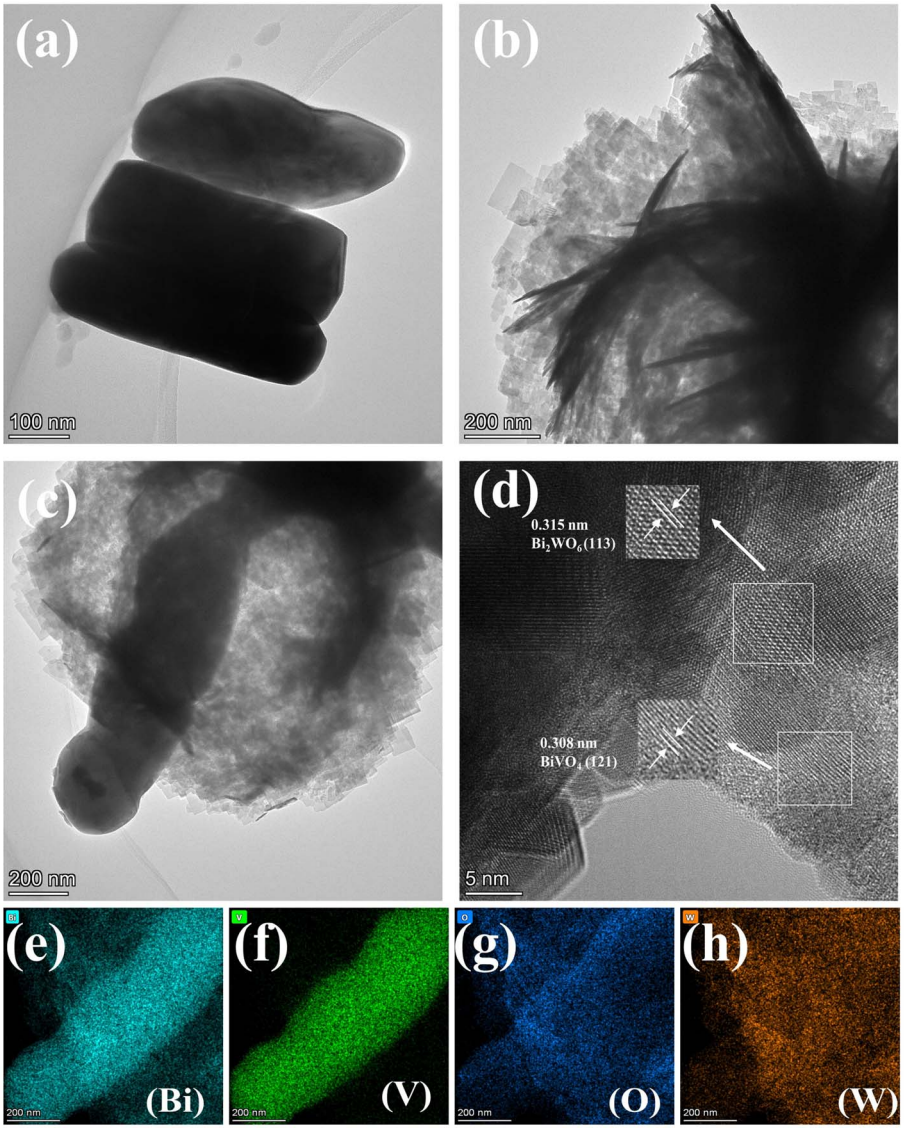

Fig. 3 TEM spectrum of (a) $BiVO_4$, (b) Bi_2WO_6 and (c) 10% W/BVO composites, (d) HRTEM spectrum of 10% W/BVO, elemental mapping of Bi (e), V (f), O (g), W (h), for 10% W/BVO.

peak of $BiVO_4$, because the proportion of the composite Bi_2WO_6 was small.[26] The diffraction peaks of (113) and (200) representing Bi_2WO_6 appeared at $2\theta = 28.3°$, 32.8°. The (011) crystal plane of the $Bi_2WO_6/BiVO_4$ composite is slightly displaced, which may be due to the formation of a heterogeneous structure.[36] In addition, two characteristic peaks at about 29° in the $Bi_2WO_6/BiVO_4$ composite are also displaced, which may be due to the overlap of the same peak positions.[37]

3.1.2 SEM analysis. The prepared materials were characterized by SEM. Fig. 2a shows that the size of pure $BiVO_4$ varies, and the morphology includes a rod-like structure. Fig. 2b shows that the morphology of Bi_2WO_6 is an irregular nano flower structure stacked by a single small nano sheet. After recombination, the nano flower-like structure of Bi_2WO_6 is destroyed, and small nano sheets are unevenly dispersed on the rod-like $BiVO_4$ (Fig. 2c).

3.1.3 TEM analysis. The sample morphology and structure were further investigated by TEM and HRTEM. Fig. 3a shows the rod-like structure of $BiVO_4$. Bi_2WO_6 in Fig. 3b shows a nanoflake structure composed of irregular flakes. In addition, Bi_2WO_6 nano sheets can be observed stacked with $BiVO_4$ in Fig. 3c, which is basically consistent with the SEM results. Fig. 3d shows the HRTEM images of 10% W/BVO with the crystal plane stripe spacing of 0.315 nm and 0.308 nm, corresponding to the (113) crystal plane of Bi_2WO_6 and the (121) crystal plane of $BiVO_4$, respectively. It was further demonstrated that Bi_2WO_6 and $BiVO_4$ form a heterojunction structure rather than a simple physical mixing.[38] In addition, the elemental mapping (Fig. 3e–h) results confirm the coexistence and homogeneous distribution of Bi, V, O and W elements in the 10% W/BVO composites.

3.1.4 XPS analysis. XPS was used to analyze the surface element composition and chemical state of materials. As shown

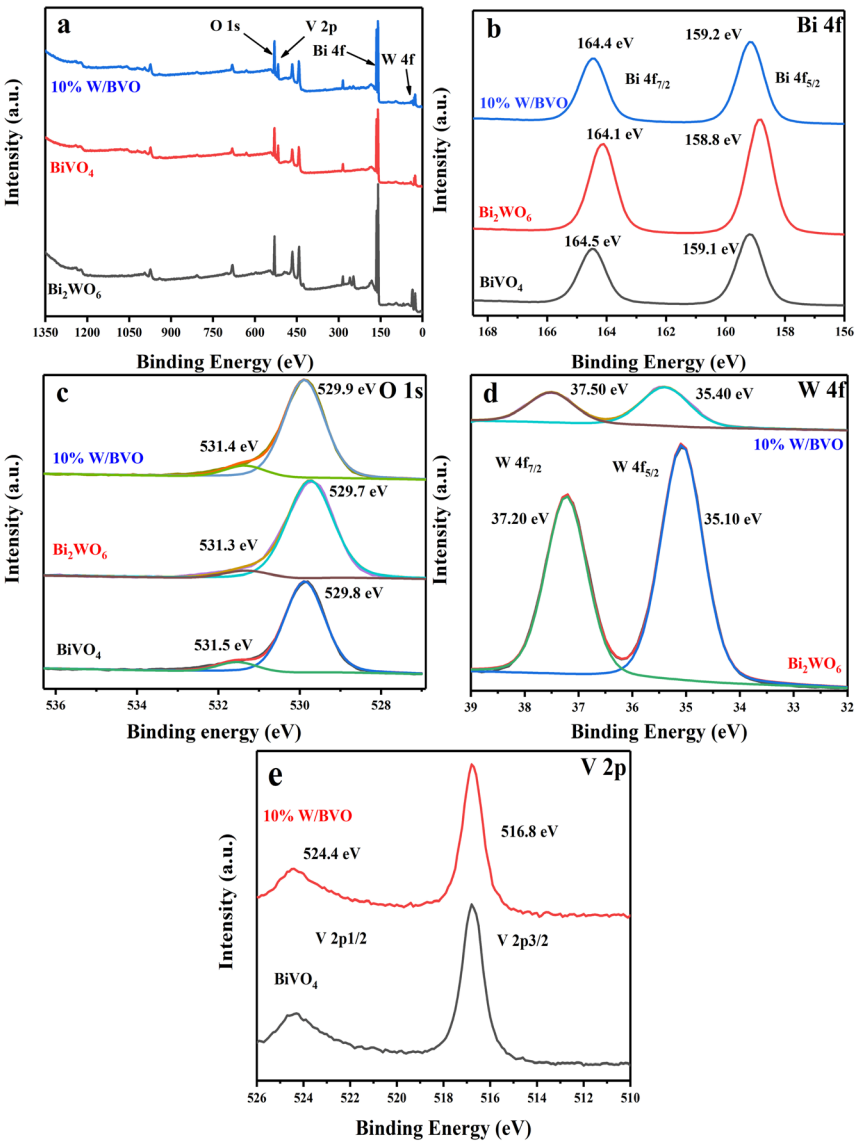

Fig. 4 (a) XPS total spectra, (b) Bi 4f, (c) O 1s, (d) W 4f, and (e) V 2p spectra of different materials.

in Fig. 4a, the full spectrum of 10% W/BVO shows the main peaks of C 1s, W 4f, V 2p, O 1s, and Bi 4f. C 1s is the external pollution carbon source. Fig. 4b shows the Bi 4f spectra of the three. The two characteristic peaks at 159.2 and 164.4 eV correspond to the Bi $4f_{5/2}$ and Bi $4f_{7/2}$ orbitals in the 10% W/BVO, respectively, indicating that the bismuth species in 10% W/BVO is Bi^{3+}.[38–40] Both were different from $BiVO_4$ and Bi_2WO_6, possibly because they were not simply physically mixed, but they also formed a heterojunction structure.[41] Fig. 4c shows that the positions of the characteristic peaks of O 1s of the three differed. After peak fitting, the peak at about 530 eV represented Bi–O lattice oxygen,[42–44] and the peak at about 531 eV represented chemisorbed oxygen.[45,46] In the characteristic peaks of W 4f (Fig. 4d), compared with the simple Bi_2WO_6, the binding energy of the characteristic peaks in 10% W/BVO had a significant red shift. W $4f_{5/2}$ and W $4f_{7/2}$ shifted from 35.1 and 37.2 eV to 35.4 and 37.5 eV, respectively, which also indicated that an interaction occurred between $BiVO_4$ and Bi_2WO_6, thus affecting the position of the characteristic peaks of W 4f.[47] Fig. 4e shows the XPS spectra of V 2p, the peaks at 516.8 eV and 524.4 eV correspond to V $2p_{3/2}$ and V $2p_{1/2}$, respectively, indicating the presence of V^{5+} in $BiVO_4$.[41,48]

3.1.5 UV-vis DRS analysis. The photocatalytic activity of the semiconductor depends on the light absorption properties of the semiconductor, and the light absorption properties of different samples were shown in Fig. 5a. Pure Bi_2WO_6 has good absorption in the UV range, poor absorption in the visible range and showed a light absorption edge at 411 nm. In the UV-vis spectrum of 10% W/BVO, it can be seen that the light absorption range of 10% W/BVO appeared red-shifted compared to pure Bi_2WO_6 due to the presence of pure $BiVO_4$, and the light absorption edge appeared at 513 nm, which was due to the good absorption ability of $BiVO_4$ in the visible range. The light absorption range of 10% W/BVO is not much different from that

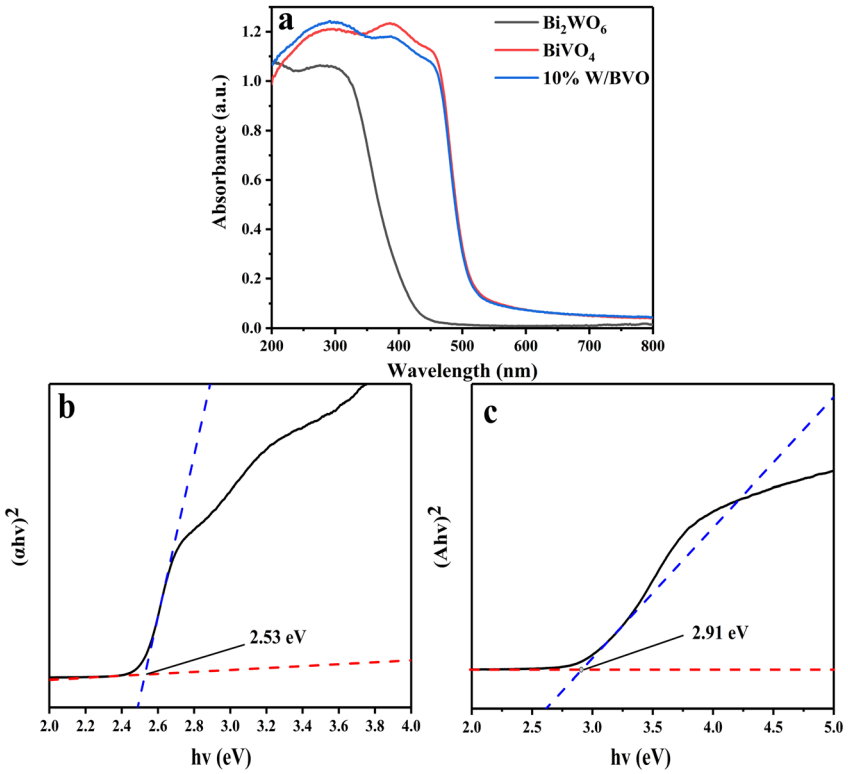

Fig. 5 (a) UV-vis spectra of different materials, (b) band gap width of $BiVO_4$, and (c) band gap width of Bi_2WO_6.

of $BiVO_4$, indicating that a small amount of Bi_2WO_6 does not affect the light absorption ability of $BiVO_4$. The band gap energy of the semiconductor was calculated by Kubelka–Munk function (eqn S(2)†), and the energy band position of the semiconductor was calculated by eqn S(3) and S(4).† [49,50] The results are shown in Fig. 5b and c and Table S1.†

3.2 Study on degradation of OTC/TC

Fig. 6 shows the photocatalytic degradation ability of different materials for tetracyclines. Fig. 6a and b show that compared with the adsorption effect under light and dark conditions without a catalyst, the system with a catalyst had obvious degradation effects on OTC and TC. Among them, Bi_2WO_6/$BiVO_4$ heterojunction significantly improved the degradation effect of OTC. When the proportion of Bi_2WO_6 was 10%, the degradation rate was the best, reaching 96.7%. When the proportion of Bi_2WO_6 continued to increase, the degradation rate started to decrease. This finding may be due to excessive Bi_2WO_6 hindered the response of $BiVO_4$ to visible light, reducing the generation rate of photogenerated charge. The degradation of TC also followed this rule. Pseudo first-order kinetics of the degradation process (Fig. 6c and d) was conducted to calculate the degradation rate constant (k). The k values of OTC degraded by $BiVO_4$, Bi_2WO_6 and 10% W/BVO were 0.0389, 0.0189 and 0.1176, respectively, and the k values of TC degraded by $BiVO_4$, Bi_2WO_6 and 10% W/BVO were 0.0654, 0.0147 and 0.0925. This shows that the photocatalytic efficiency of Bi_2WO_6/$BiVO_4$ composite was significantly better than those of the two materials alone.

In order to investigate the application of the catalyst in the real water environment, Na_2SO_4, $NaNO_3$, $NaHCO_3$ and NaCl were added to investigate the effect of different anions on the photodegradation effect. As shown in Fig. 7, the degradation efficiency of OTC was slightly inhibited by the addition of anions, and the inhibition effect was NO_3^- > SO_4^{2-} > Cl^- > HCO_3^- in order. This may be due to the fact that anions can adsorb on the active sites on the material surface, thus reducing the contact between the material and the pollutant and affecting its degradation effect.[51,52] Alternatively, the anions may directly consume the active groups produced by photocatalysis, leading to a decrease in OTC degradation efficiency.[53–55]

To study the stability and reuse performance of the photocatalyst, the recycling experiments of the 10% W/BVO composite were carried out. As shown in Fig. 8, after five repeated photocatalytic experiments, the degradation rate of 10% W/BVO composites for OTC under visible light did not decrease significantly, indicating that the Bi_2WO_6/$BiVO_4$ composite catalyst has excellent stability and reusability, and is practical for wide use in the field of environmental remediation.

To explore the types of main active free radicals in the process of OTC/TC degradation, different quenching agents were added to the system to prevent the action of active groups. As shown in Fig. 9, in the process of OTC degradation, the addition of HCOOH (h^+ quenching agent) or the reaction in N_2 atmosphere (inhibition of $\cdot O_2^-$ production)[56] significantly inhibited the degradation effect, whereas the addition of isopropanol (*t*-butanol, ·OH inhibitor) achieved 93.7% of the degradation effect. This was only 3.0% lower than that without

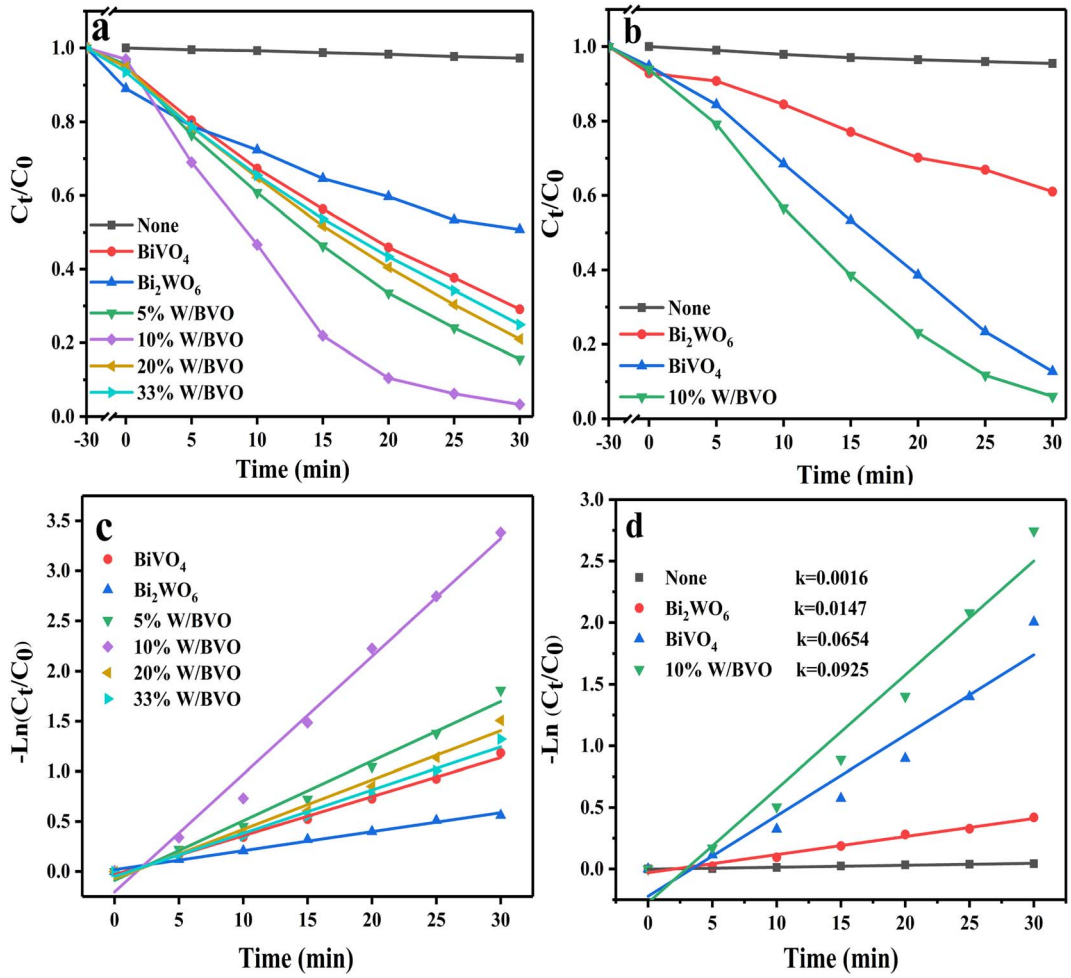

Fig. 6 (a) Photocatalytic degradation of OTC and (c) pseudo first order dynamic fitting model, (b) photocatalytic degradation of TC for different materials and (d) pseudo first order dynamic fitting model.

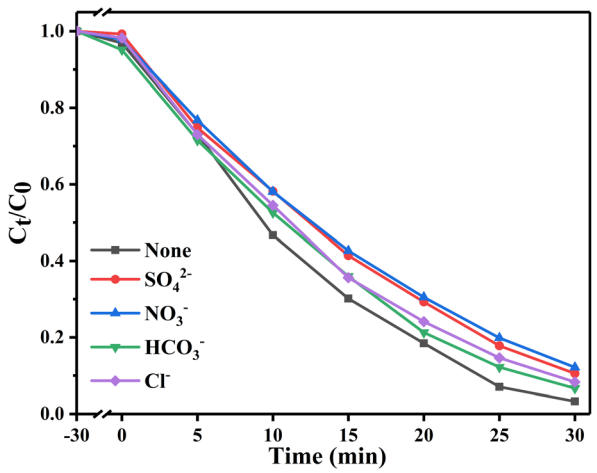

Fig. 7 Photocatalytic degradation of OTC under different ions.

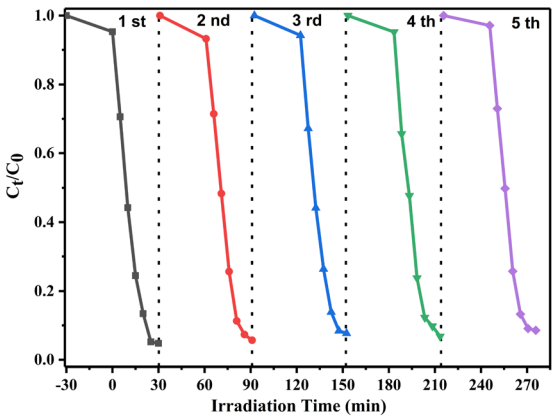

Fig. 8 Cycling runs of 10% W/BVO for OTC degradation under visible light.

quenching agent. This finding showed that h^+ and $\cdot O_2^-$ played a major role in the photocatalytic degradation of OTC, whereas ·OH did not play a significant role.

The active species in the photocatalytic reaction was further demonstrated by the ESR spin trap technique using 5,5-dimethyl-1-pyrroline-*N*-oxide (DMPO) as the active species trap to produce stable DMPO-$\cdot O_2^-$ and DMPO-·OH in methanol and

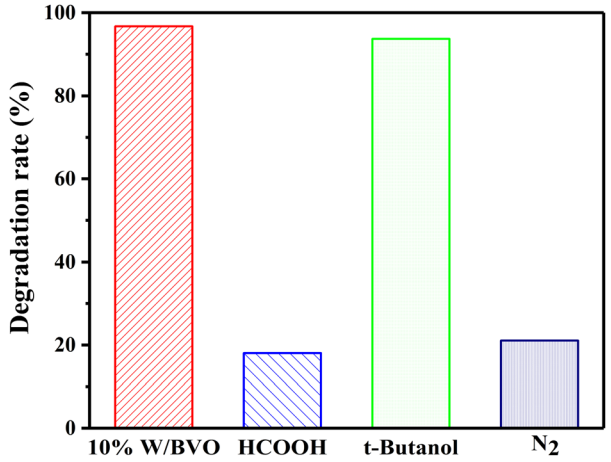

Fig. 9 Photocatalytic degradation of OTC free radical capture experiment.

aqueous humor, respectively. As shown in Fig. 10a, the characteristic peak of DMPO-·O_2^- appears under visible light irradiation, indicating the generation of ·O_2^-, and the highest intensity of DMPO-·O_2^- peak generated by 10% W/BVO was due to the formation of heterojunction to promote charge separation and the photogenerated electron reduction of O_2 to produce more ·O_2^-.[57] In addition, the characteristic peaks of DMPO-·OH were shown in Fig. 10b, and the intensity of DMPO-·OH peaks generated by 10% W/BVO was significantly higher than that of pure Bi_2WO_6 and $BiVO_4$, indicating that 10% W/BVO can generate more ·OH.

The system had an obvious degradation effect on OTC and TC, and the key was the ability of electron migration between the system interfaces. To verify the separation efficiency of photogenerated carriers, PL spectra and transient photocurrent at 295 nm were measured. Fig. 11a shows that the relative intensity of PL spectrum was in the following order: Bi_2WO_6 > $BiVO_4$ > 10% W/BVO, which suggested that the recombination efficiency of

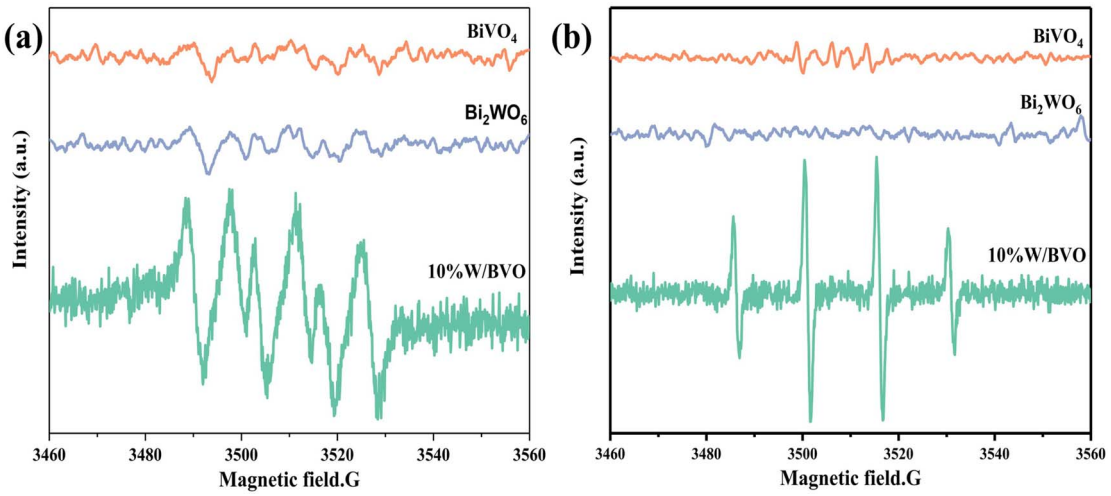

Fig. 10 DMPO ESR spectra under visible light for 10 min: (a) in methanol dispersion for DMPO-·O_2^- and (b) in aqueous dispersion for DMPO-·OH.

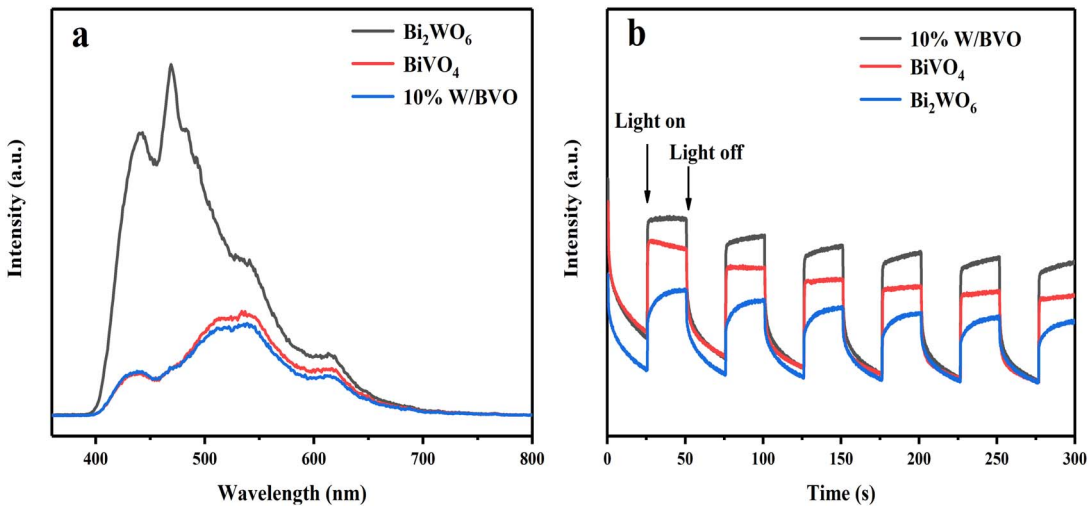

Fig. 11 (a) Photoluminescence spectra of different materials and (b) transient photocurrent response spectra.

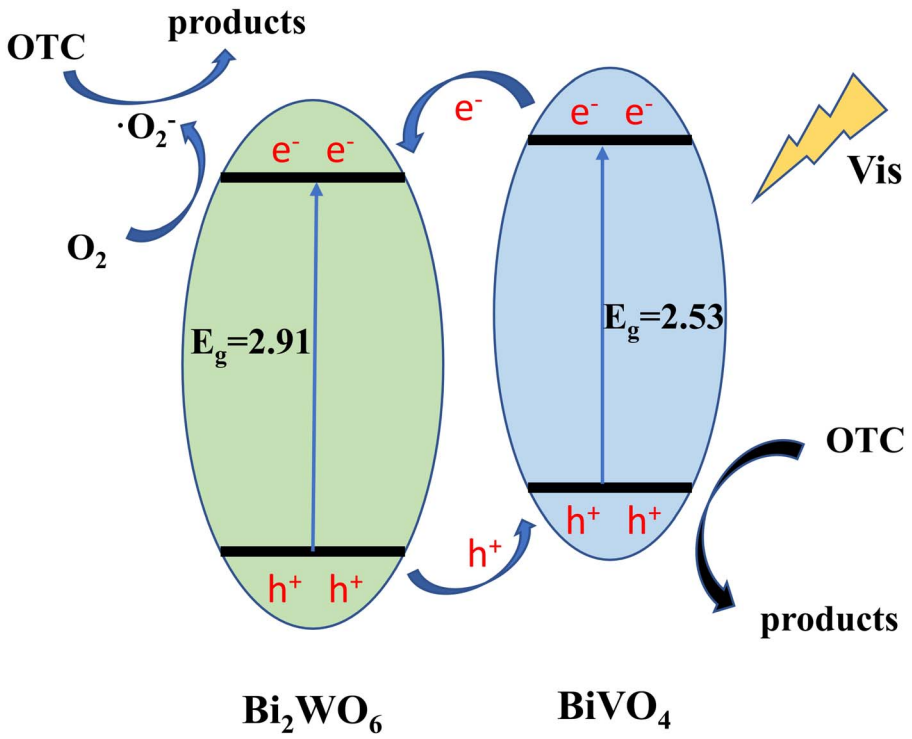

Fig. 12 Mechanism of $Bi_2WO_6/BiVO_4$ photocatalytic performance improvement.

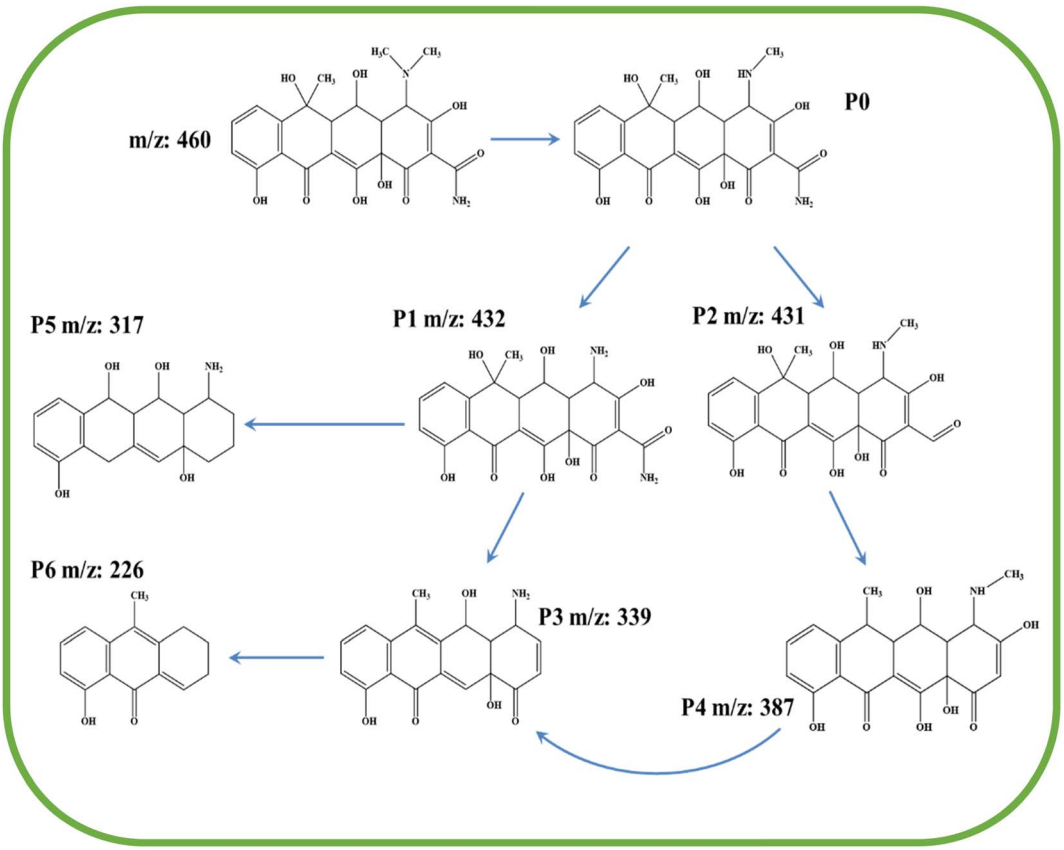

Fig. 13 Possible degradation path of OTC.

photogenerated carriers of 10% W/BVO was lower. The transient photocurrent response spectrum (Fig. 11b) showed that the relative photocurrent intensity of 10% W/BVO was higher than that of Bi_2WO_6 and $BiVO_4$ after the lamp was turned on, indicating that the carrier migration efficiency in 10% W/BVO was better, which was also consistent with the PL spectral analysis results.

Through the above characterization analysis and radical trapping experiments, the mechanism of efficient OTC removal by $Bi_2WO_6/BiVO_4$ was proposed. The energy band structure of Bi_2WO_6 and $BiVO_4$ formed a type II heterojunction structure, which facilitates the separation rate of photogenerated charges. As shown in Fig. 12, both $BiVO_4$ and Bi_2WO_6 produce photogenerated holes (h^+) and photogenerated electrons (e^-) with charge redistribution when visible light was irradiated onto the composite surface. Considering that the E_{CB} of Bi_2WO_6 (+0.41 V *vs.* NHE) was lower than that of $BiVO_4$ (+0.39 V *vs.* NHE), the e^- of $BiVO_4$ can be transferred to the surface of Bi_2WO_6 under thermodynamic driving force. The e^- on the conduction band of Bi_2WO_6 can react with the oxygen molecules adsorbed on the surface to form $\cdot O_2^-$ in a reduction reaction.[58] Similarly, the E_{VB} of $BiVO_4$ (+2.91 V *vs.* NHE) was higher than that of Bi_2WO_6 (+3.32 V *vs.* NHE), and the h^+ formed by Bi_2WO_6 can be transferred to the $BiVO_4$ surface. The formed $\cdot O_2^-$ and h^+ reacted with the OTC adsorbed on the surface of the material by oxidation, and the OTC degrades to form small molecules. Since the e^- and h^+ at the interface of Bi_2WO_6 and $BiVO_4$ were effectively separated, it was conducive to reducing the compounding chance and thus improving the photocatalytic activity of the system.

3.3 Analysis of OTC degradation path

The paper further explored the degradation path of OTC by 10% W/BVO by analyzing the intermediates produced in the degradation process. The original LC-MS plot of OTC degradation intermediates was shown in Fig. S1.† Table S2† shows the specific substances detected. Fig. 13 shows the possible degradation pathway of OTC based on LC-MS analysis results. **P1** (m/z = 432) was the product of the removal of two methyl groups from the C–N bond in N–CH_3 due to the attack of active free radicals, and the removal of one methyl group was **P0**. **P2** (m/z = 431) was the product of C–N deamination in **P0**.[59] **P4** (m/z = 387) was the product of decarbonylation and hydroxylation of **P2**. Two production paths for **P3** (m/z = 339) existed. One was the product of **P1** dehydroxylation and amide, and the other was the product of **P4** demethylation and hydroxyl. **P5** (m/z = 317) may be the product of **P1** demethylation, amide, and hydroxyl that can destroy the carbonyl group. **P6** (m/z = 226) may be the intermediate obtained from the dehydroxylation of **P3**.[60] The base peak in the mass spectrum of **P6** was excimer ion (2M + H).

4. Conclusions

$Bi_2WO_6/BiVO_4$ composites were synthesized for the photocatalytic degradation of OTC/TC. XRD, SEM, XPS, UV-Vis DRS, PL and photocurrent were used to study the structure, morphology, surface chemical state and photoelectric properties of the materials. The influence of common anions in water on OTC degradation was investigated. The reaction mechanism and OTC degradation path were also preliminarily explored, and the following conclusions were obtained:

(1) Compared with single $BiVO_4$ and Bi_2WO_6, the construction of $Bi_2WO_6/BiVO_4$ heterojunction system significantly improved the efficiency of photocatalytic removal of OTC/TC. The removal rate of OTC by 10% W/BVO photocatalyst reached 96.7%, and the degradation rate were 6.22 and 3.02 times that of Bi_2WO_6 and $BiVO_4$ respectively.

(2) Common anions can inhibit the degradation efficiency of OTC to varying degrees in the following order: $NO_3^- > SO_4^{2-} > Cl^- > HCO_3^-$.

(3) The formation of heterojunctions promoted the separation rate of photogenerated charges and improved the photocatalytic activity.

(4) The free radical quenching experiment showed that $\cdot O_2^-$ and h^+ play a major role in the process of OTC degradation. High resolution mass spectrometry analysis showed that there were six intermediates in the reaction process, and the possible degradation path was speculated.

Author contributions

Yiyao Zhang: resources, software, methodology, writing – original draft. Hongchen Song: resources, data curation, software, writing – original draft. Jintai Han: formal analysis, supervision. Yunchao Liu: visualization. Jing Sun: resources, funding acquisition, formal analysis, supervision. Tingting Shen: funding acquisition, validation, data curation. Xikui Wang: project administration, investigation. Zhen Wang: formal analysis. Weizhen Zhang: investigation. Xuerui Yao: data curation.

Conflicts of interest

The authors declare no conflict of interest.

Acknowledgements

This research was supported by the Qilu University of Technology (Shandong Academy of Sciences) Basic Research Project of Science, Education and Industry Integration Pilot Project (2022PY047).

Notes and references

1 J. Wu, J. Hu, H. Qian, J. Li, R. Yang and L. Qu, *Diamond Relat. Mater.*, 2022, **121**, 108738.
2 M. Wang, C. Jin, J. Kang, J. Liu, Y. Tang, Z. Li and S. Li, *Chem. Eng. J.*, 2021, **416**, 128118.
3 Y. Dai, Y. Liu, J. Kong, J. Yuan, C. Sun, Q. Xian, S. Yang and H. He, *Solid State Sci.*, 2019, **96**, 105946.
4 W. Wang, Q. Han, Z. Zhu, L. Zhang, S. Zhong and B. Liu, *Advanced Powder Technology*, 2019, **30**, 1882–1896.
5 S. Wang, J. Li, C. Wang, J. Ma, Z. Li, Z. Zheng and J. Zhang, *Bioresour. Technol.*, 2022, **348**, 126756.
6 C. Zhao, Y. Zhou, D. J. d. Ridder, J. Zhai, Y. Wei and H. Deng, *Chem. Eng. J.*, 2014, **248**, 280–289.

7 K. Zhou, X.-D. Xie and C.-T. Chang, *Appl. Surf. Sci.*, 2017, **416**, 248–258.
8 Z. Lu, J. Peng, M. Song, Y. Liu, X. Liu, P. Huo, H. Dong, S. Yuan, Z. Ma and S. Han, *Chem. Eng. J.*, 2019, **360**, 1262–1276.
9 V. K. Sharma, N. Johnson, L. Cizmas, T. J. McDonald and H. Kim, *Chemosphere*, 2016, **150**, 702–714.
10 L. Chen, C. W. Chen, C. P. Huang, Y. Chuang, T. B. Nguyen and C. D. Dong, *J. Colloid Interface Sci.*, 2022, **616**, 67–80.
11 S. Zhang, S. Zhao, S. Huang, B. Hu, M. Wang, Z. Zhang, L. He and M. Du, *Chem. Eng. J.*, 2021, **420**, 130516.
12 A. S. Oberoi, Y. Jia, H. Zhang, S. K. Khanal and H. Lu, *Environ. Sci. Technol.*, 2019, **53**, 7234–7264.
13 M. B. Ahmed, J. L. Zhou, H. H. Ngo, W. Guo, N. S. Thomaidis and J. Xu, *J. Hazard. Mater.*, 2017, **323**, 274–298.
14 G. Liao, Y. Gong, L. Zhang, H. Gao, G.-J. Yang and B. Fang, *Energy Environ. Sci.*, 2019, **12**, 2080–2147.
15 G. Liao, C. Li, X. Li and B. Fang, *Cell Rep. Phys. Sci.*, 2021, **2**, 100355.
16 Z. Du, L. Feng, Z. Guo, T. Yan, Q. Hu, J. Lin, Y. Huang, C. Tang and Y. Fang, *J. Colloid Interface Sci.*, 2021, **589**, 545–555.
17 Y. Li, Z. Lai, Z. Huang, H. Wang, C. Zhao, G. Ruan and F. Du, *Appl. Surf. Sci.*, 2021, **550**, 149342.
18 H. Tang, W. Zhang, Y. Meng and S. Xia, *Appl. Catal., B*, 2021, **285**, 119851.
19 Q. Zhang, L. Jiang, J. Wang, Y. Zhu, Y. Pu and W. Dai, *Appl. Catal., B*, 2020, **277**, 119122.
20 C. Zhao, H. Deng, Y. Li and Z. Liu, *J. Hazard. Mater.*, 2010, **176**, 884–892.
21 F. Chang, J. Zhang, Y. Xie, J. Chen, C. Li, J. Wang, J. Luo, B. Deng and X. Hu, *Appl. Surf. Sci.*, 2014, **311**, 574–581.
22 F. Chang, Y. Xie, C. Li, J. Chen, J. Luo, X. Hu and J. Shen, *Appl. Surf. Sci.*, 2013, **280**, 967–974.
23 N. Dang Phu, L. Huy Hoang, P.-C. Guo, X.-B. Chen and W. Ching Chou, *J. Sol-Gel Sci. Technol.*, 2017, **83**, 640–646.
24 M. Zhang, J. Lu, C. Zhu, Y. Xiang, L. Xu and T. Chen, *Solid State Sci.*, 2019, **90**, 76–85.
25 Y. L. Geng, P. Zhang and S. P. Kuang, *RSC Adv.*, 2014, **4**, 46054–46059.
26 X. Zhang, Y. Gong, X. Dong, X. Zhang, C. Ma and F. Shi, *Mater. Chem. Phys.*, 2012, **136**, 472–476.
27 T. Saison, N. Chemin, C. Chanéac, O. Durupthy, V. Ruaux, L. Mariey, F. Maugé, P. Beaunier and J.-P. Jolivet, *J. Phys. Chem. C*, 2011, **115**, 5657–5666.
28 C. Chen, J. Hu, X. Yang, T. Yang, J. Qu, C. Guo and C. M. Li, *ACS Appl. Mater. Interfaces*, 2021, **13**, 20162–20173.
29 T. Yang, Y. Shao, J. Hu, J. Qu, X. Yang, F. Yang and C. Ming Li, *Chem. Eng. J.*, 2022, **448**, 137613.
30 P. Ju, P. Wang, B. Li, H. Fan, S. Ai, D. Zhang and Y. Wang, *Chem. Eng. J.*, 2014, **236**, 430–437.
31 J. Hu, C. Chen, Y. Zheng, G. Zhang, C. Guo and C. M. Li, *Small*, 2020, **16**, e2002988.
32 W. Wang, L. Lin, D. Yu and B. Liu, *J. Nanosci. Nanotechnol.*, 2018, **18**, 7691–7702.
33 Y. Geng, P. Zhang and S. Kuang, *RSC Adv.*, 2014, **4**, 46054–46059.
34 S. Chaiwichian, B. Inceesungvorn, K. Wetchakun, S. Phanichphant, W. Kangwansupamonkon and N. Wetchakun, *Mater. Res. Bull.*, 2014, **54**, 28–33.
35 S. Luo, J. Ke, M. Yuan, Q. Zhang, P. Xie, L. Deng and S. Wang, *Appl. Catal., B*, 2018, **221**, 215–222.
36 Q. Chi, G. Zhu, D. Jia, W. Ye, Y. Wang, J. Wang, T. Tao, F. Xu, G. Jia, W. Li and P. Gao, *Nanoscale*, 2021, **13**, 4496–4504.
37 K. Shahzad, M. B. Tahir and M. Sagir, *Appl. Nanosci.*, 2020, **10**, 2037–2043.
38 P. Ju, Y. Wang, Y. Sun and D. Zhang, *Dalton Trans.*, 2016, **45**, 4588–4602.
39 L. Chen, D. Meng, X. Wu, A. Wang, J. Wang, M. Yu and Y. Liang, *RSC Adv.*, 2016, **6**, 52300–52309.
40 Z. Liu, X. Liu, L. Wei, C. Yu, J. Yi and H. Ji, *Appl. Surf. Sci.*, 2020, **508**, 145309.
41 S. Chaiwichian, K. Wetchakun, S. Phanichphant, W. Kangwansupamonkon and N. Wetchakun, *RSC Adv.*, 2016, **6**, 54060–54068.
42 L. Ji, L. Lin, D. Yu, P. Gao, W. Wang and B. Liu, *Mater. Lett.*, 2018, **220**, 94–98.
43 S. Jonjana, A. Phuruangrat, S. Thongtem and T. Thongtem, *Mater. Lett.*, 2018, **216**, 92–96.
44 X. Yuan, D. Shen, Q. Zhang, H. Zou, Z. Liu and F. Peng, *Chem. Eng. J.*, 2019, **369**, 292–301.
45 J. Zhang, H. Cui, B. Wang, C. Li, J. Zhai and Q. Li, *Appl. Surf. Sci.*, 2014, **300**, 51–57.
46 Y. Liu, L. Huang, Y. Fang, X. Zhu and S. Dong, *Nano Res.*, 2021, **14**, 2711–2716.
47 H. Hu, W. Kong, J. Wang, C. Liu, Q. Cai, Y. Kong, S. Zhou and Z. Yang, *Appl. Surf. Sci.*, 2021, **557**, 149796.
48 H.-b. Li, J. Zhang, G.-y. Huang, S.-h. Fu, C. Ma, B.-y. Wang, Q.-r. Huang and H.-w. Liao, *Trans. Nonferrous Met. Soc. China*, 2017, **27**, 868–875.
49 J. Hu, X. Li, J. Qu, X. Yang, Y. Cai, T. Yang, F. Yang and C. M. Li, *Chem. Eng. J.*, 2023, **453**, 139957.
50 J. Hu, C. Chen, H. Yang, F. Yang, J. Qu, X. Yang, W. Sun, L. Dai and C. M. Li, *Appl. Catal., B*, 2022, **317**, 121723.
51 Y. Li, J. Wang, H. Yao, L. Dang and Z. Li, *J. Mol. Catal. A: Chem.*, 2011, **334**, 116–122.
52 C. Chang, H. Yang, L. Kan, W. Mu, Q. Wang, S.-Y. Lu and B. Deng, *J. Taiwan Inst. Chem. Eng.*, 2021, **125**, 176–185.
53 C. Lai, F. Huang, G. Zeng, D. Huang, L. Qin, M. Cheng, C. Zhang, B. Li, H. Yi, S. Liu, L. Li and L. Chen, *Chemosphere*, 2019, **224**, 910–921.
54 C. Hu, J. C. Yu, Z. Hao and P. K. Wong, *Appl. Catal., B*, 2003, **46**, 35–47.
55 B. Ma, S. Xin, X. Ma, C. Zhang and M. Gao, *Appl. Surf. Sci.*, 2021, **551**, 149480.
56 Y. Zhu, Y. Wang, W. Yao, R. Zong and Y. Zhu, *RSC Adv.*, 2015, **5**, 29201–29208.
57 X. a. Dong, W. Zhang, Y. Sun, J. Li, W. Cen, Z. Cui, H. Huang and F. Dong, *J. Catal.*, 2018, **357**, 41–50.
58 Y. Zhou, Y. Zhang, M. Lin, J. Long, Z. Zhang, H. Lin, J. C. Wu and X. Wang, *Nat. Commun.*, 2015, **6**, 8340.
59 Q. Chen, S. Wu and Y. Xin, *Chem. Eng. J.*, 2016, **302**, 377–387.
60 J. Xu, Z. Bian, X. Xin, A. Chen and H. Wang, *Chem. Eng. J.*, 2018, **337**, 684–696.